Cyclotron-resonance-assisted photon drag effect in InSb/InAlSb quantum wells excited by terahertz radiation

S Stachel,[1] G V Budkin,[2] U Hagner,[1] V V Bel'kov,[2] M M Glazov,[2]
S A Tarasenko,[2] S K Clowes,[3] T Ashley,[4] A M Gilbertson,[5] and S D Ganichev[1]
[1] *Terahertz Center, University of Regensburg, 93040 Regensburg, Germany*
[2] *Ioffe Physical-Technical Institute, Russian Academy of Sciences, 194021 St. Petersburg, Russia*
[3] *Advanced Technology Institute and SEPNet, University of Surrey, Surrey GU2 7XH, UK*
[4] *School of Engineering, University of Warwick, Coventry CV4 7AL, UK and*
[5] *Blackett Laboratory, Imperial College, London SW7 2BZ, UK*

We report on the observation of the cyclotron-resonance-assisted photon drag effect. Resonant photocurrent is detected in InSb/InAlSb quantum wells structures subjected to a static magnetic field and excited by terahertz radiation at oblique incidence. The developed theory based on Boltzmann's kinetic equation is in a good agreement with the experimental findings. We show that the resonant photocurrent originates from the transfer of photon momentum to free electrons drastically enhanced at cyclotron resonance.

PACS numbers: 72.40.+w, 73.21.Fg, 73.50.Jt

INTRODUCTION

Indium antimonide based quantum well (QW) structures exhibiting the highest room temperature electron mobility of any semiconductors are considered as a prospective material for the next generation of electronic devices being of particular interest for such applications as high mobility transistors [1] and ballistic transport based electronics. [2–4] Apart from the high mobility caused by the small effective electron mass, these nanostructures are also characterized by large dielectric constant, enhanced Landé g-factor and a strong spin-orbit coupling, [5–7] making them particularly interesting for the studies of spin physics. Whereas electronic transport in InSb/AlInSb heterostructures has been investigated in depth, less is known about their optoelectronic properties. At the same time, already the first experiments have demonstrated that the photocurrents excited by infrared/terahertz radiation give an access to the Rashba spin-splitting of the conduction band [8], results in a spin-dependent electron transport [9–11], prove the high polarization-dependent spin susceptibility and enhanced electron-electron exchange interaction [9]. Photoelectric effects have been also shown to be an effective way to inject spin polarized electric currents and to study the anisotropy of the band spin-splitting [12]. Being caused by the absorption of electromagnetic radiation, photocurrent generation efficiency can be strongly enhanced under resonant absorption conditions. In particular, cyclotron resonance (CR) serves as an effective tool to magnify the photoresponse. Textbook CR experiments on bulk InSb crystals excited by terahertz radiation[13] and more recent results on InSb-based QWs[14–16] reveal that the radiation absorption can be increased tenfold and CR, due to very small effective mass, emerges at low magnetic field of a few Tesla.

Here, we report on the observation and detailed study of the cyclotron-resonance-assisted photocurrent induced by terahertz laser radiation in InSb/AlInSb QWs. We show that, in (001)-grown QWs, the photocurrent can be excited at oblique incidence only. Applying radiation with the frequency of about 2.5 THz, the photocurrent enhancement by more than 50 times is detected at the magnetic field of about 2 T as compared to the photocurrent excited at zero field. Both the resonance position and the enhancement factor correlate well with those of the optical transmission measurements clearly indicating the CR absorption. The developed theory, being in a good agreement with experimental findings, demonstrates that the electric current originates from the transfer of photon momentum to free electrons, that is the photon-drag effect.

SAMPLES AND EXPERIMENTAL TECHNIQUES

The experiments are carried out on 30 nm wide InSb QW structures grown on (001)-oriented semi-insulting GaAs substrates by molecular beam epitaxy. The lower barrier of the well consists of $In_{0.9}Al_{0.1}Sb$ while the top barrier is $In_{0.85}Al_{0.15}Sb$ containing a Te δ-doping layer. The QW hosts a two-dimensional electron gas (2DEG) with a carrier density of $n_s = 5 \times 10^{11}\,\mathrm{cm}^{-2}$ and a mobility of $\mu = 1 \times 10^5$ cm^2/Vs at 77 K. The samples are square shaped with a length of 5 mm. The sample edges are oriented along the $x \parallel [1\bar{1}0]$ and $y \parallel [110]$ crystallographic axes. Four ohmic contacts fabricated at the middle of each sample edge allow us to probe the photocurrent in x- and y-directions (see the inset in Fig. 1).

To generate photocurrents in unbiased samples we applied *cw* or pulsed terahertz (THz) laser systems. As a source of *cw* radiation, a CH_3OH laser [17] operating at the frequency 2.54 THz (photon energies $\hbar\omega = 10.4$ meV) was used. The incident power $P \approx 0.5$ mW at the sam-

ple was modulated at 800 Hz by an optical chopper. The radiation at oblique incidence was focused in a spot of about 1.5 mm diameter at the center of sample. The spatial beam distribution had an almost Gaussian profile which was measured by a pyroelectric camera.[18] The electric field $\boldsymbol{E}$ of linearly polarized laser radiation was oriented either parallel (p-polarization) or perpendicularly (s-polarization) to the plane of incidence. Note that in the latter case, the electric field vector lied in the QW plane. For the pulsed radiation, an NH_3 laser[19, 20] operating at the frequencies $f = 1.07$, 2.03, and 3.31 THz ($\hbar\omega = 4.4$, 8.4, and 13.7 meV, respectively) was applied. The laser generates single pulses with a duration of about 100 ns, peak power of $P \approx 5$ kW, and a repetition rate of 1 Hz. The radiation power was controlled by the THz photon drag detector.[21] A typical spot diameter was from 1 to 3 mm. The beam had an almost Gaussian shape, which was measured by the pyroelectric camera.

The geometry of the experiments is sketched in the insets in Figs. 1 and 2. Samples were excited by the laser beam lying in the (xz) plane at the angle of incidence θ_0, varied between $-30°$ to $+30°$, with respect to the layer normal $z \parallel [001]$. Both the current components perpendicular, j_y, and parallel, j_x, to the plane of incidence were investigated. The corresponding photocurrents were measured by the voltage drops, $U_{x(y)}$, picked up across a 1 MΩ (cw measurements) or 50 Ω (pulsed measurements) load resistors. To record the signal in both cases, a lock-in amplifier and digital oscilloscope were applied, respectively. Complimentary transmission measurements were performed applying cw laser operating at the frequencies $f = 1.63$ or 2.54 THz and the Golay cell as a sensitive radiation detector. These measurements were done at normal incidence of radiation using linearly polarized as well as right-handed (σ^+) and left-handed (σ^-) circularly polarized light obtained by $\lambda/4$-plates. Samples were mounted in a temperature variable magneto-optical cryostat. Experiments were carried out in the temperature range between 4.2 and 120 K and the magnetic field up to 7 T applied along z-direction.

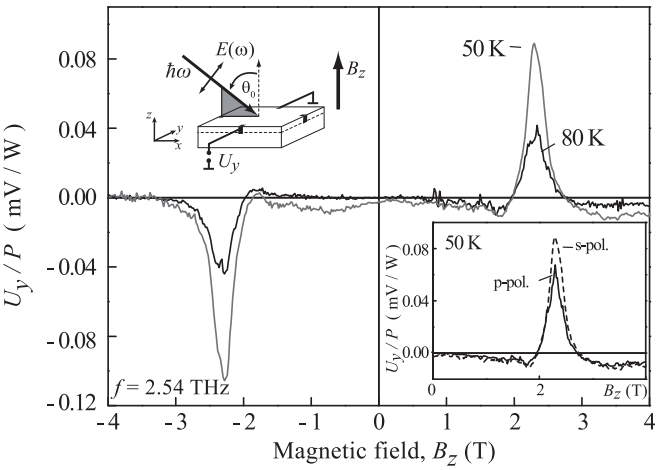

FIG. 1: Photosignal U_y normalized by the radiation power P excited by linearly polarized light (s-polarization) with f = 2.54 THz as a function of the magnetic field B_z, incidence angle $\theta_0 = 20^0$. The left inset shows the experimental geometry. The right one presents the field dependences for s- and p-polarized radiation.

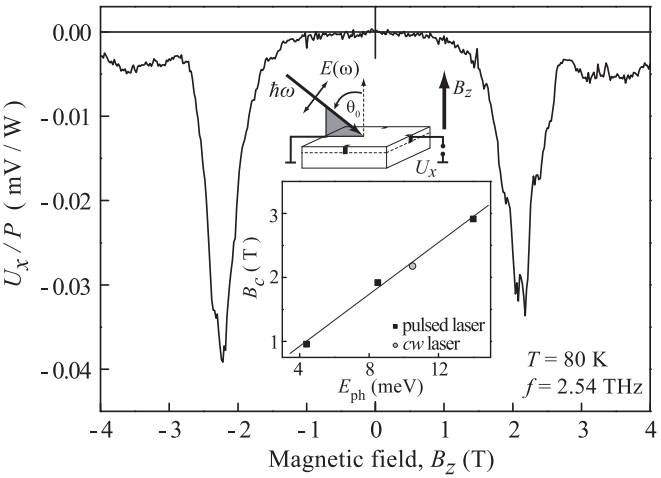

FIG. 2: Photosignal U_x normalized by the radiation power P excited by linearly polarized (p-polarization) light with f = 2.54 THz as a function of the magnetic field B_z, incidence angle $\theta_0 = 20^0$. The top inset shows the experimental geometry. The bottom one demonstrates magnetic field positions, B_c, of the resonant photosignals induced by the cw (f = 2.54 THz) and pulsed laser systems as a function of the photon energy E_{ph} obtained at $T = 4.2$ K.

RESULTS

We start with the data obtained at rather high temperatures (above ≈ 20 K) and applying low power radiation of cw laser operating at f = 2.54 THz. Exciting the sample with linearly polarized radiation at oblique incidence[22] and sweeping magnetic field, we observed a resonant photosignal with the maximum at $|B_c| = 2.3$ T, see Figs. 1 and 2. The resonant photoresponses are detected in both *perpendicular* and *parallel* to the light incident plane directions. However, the signal parities are different: In the former case (U_y) it is *odd* (Fig. 1) while in the latter case (U_x) it is *even* (Fig. 2) in the magnetic field B_z. As an important result, the magnitude of the resonances is almost independent of the orientation of the radiation electric field vector $\boldsymbol{E}_\omega$ with respect to QW plane. The photocurrents excited by the radiation polarized in the QW plane (s-polarization, $\boldsymbol{E}_\omega \parallel y$) and the field with the orthogonal polarization (p-polarization, $E_{\omega,z} \neq 0$) are shown in the inset in Fig. 1.

In the temperature range between 20 and 100 K, the resonances are well described by the Lorentz functions, whose magnitude increases with a decrease of the temper-

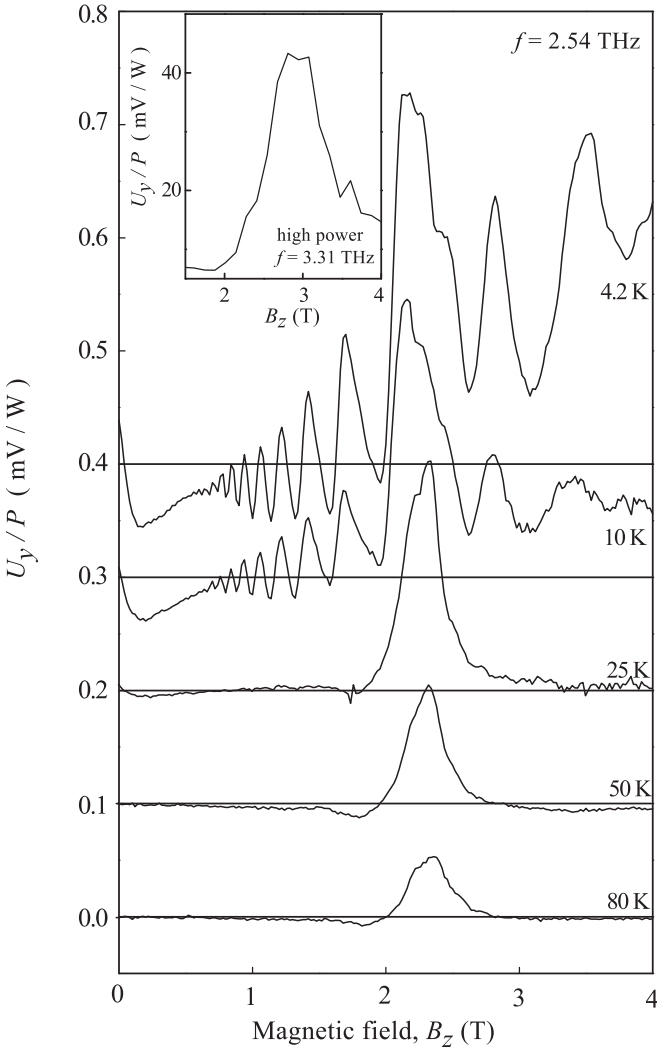

FIG. 3: Magnetic field dependence of U_y/P for linearly polarized radiation of $f = 2.54\,\mathrm{THz}$ and different temperatures T. The data for $T < 80\,\mathrm{K}$ are consistently shifted by $+0.1\,\mathrm{mV/W}$ for each step in temperature. Inset shows photovoltage resonance observed at 4.2 K under high power excitation of the pulse laser, $f = 3.31\,\mathrm{THz}$. The signal U_y in the inset is normalized by the maximum detected signals, $U_{y,max}$.

ature. For lower temperatures, $T < 20\,\mathrm{K}$, the magnetic field behavior of the photocurrent becomes more complicated. Figure 3 shows that now the photosignal oscillates upon variation of magnetic field. The amplitude of the oscillations increases with rising B_z achieves a maximum at $B_z \approx B_c$ and decreases for higher magnetic fields. Analysis of the data reveals that the oscillations are periodic with $1/B_z$. This is shown in Fig. 4 demonstrating a linear dependence of the inverse magnetic field positions, $1/B_{max}$, of the photosignal maxima on an integer index N. Additional magneto-transport measurements demonstrate that the period of the observed oscillations is twice as that of the Shubnikov-de Haas oscillations (SdH), see Fig. 4. At substantially higher radiation intensities obtained applying pulsed terahertz laser, the oscillations vanish even at low sample temperatures, see inset in Fig. 3.

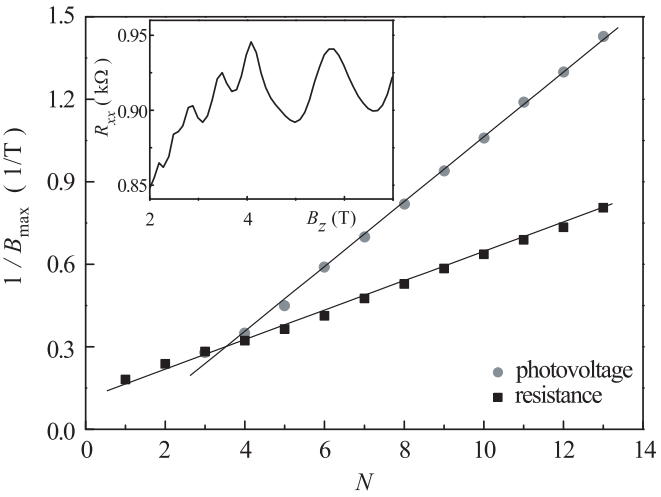

FIG. 4: Oscillation maxima of the photocurrent and SdH oscillations measured at $T = 4.2\,\mathrm{K}$ are assigned an integer index N. Their $1/B$-field positions are plotted versus the index. The inset shows the longitudinal resistance $R_{xx}(B_z)$ measured in the van der Pauw geometry for a constant current of $1\,\mu\mathrm{A}$. Note, that the SdH oscillations are superimposed by a high background signal resulting from the parallel conductance of the δ-doping layer in the AlInSb barrier which is well known for InSb/AlInSb QWs.[23, 24]

The magnetic field B_c corresponding to the resonance versus the photon energy are shown in the inset in Fig. 2. The linear scaling of B_c with the radiation frequency, almost Lorentz shape of the resonance, and the magnitudes of B_c indicate that the resonances are caused by the cyclotron absorption of radiation. This conclusion is supported by the magnetic field dependence of the radiation transmission measured for normally incident radiation of the *cw* laser. Figure 5 shows that the data obtained for linearly and circularly polarized radiation with $f = 2.54\,\mathrm{THz}$ have a characteristic cyclotron resonance behavior: While for left-handed (right-handed) polarized light the transmission shows a sharp decrease at $B_c \approx$ -2.3 T (+2.3 T) only for one magnetic field polarity, for linear polarization the dips in the transmission are observed for both magnetic field polarities and the dip magnitudes are reduced by the factor of two. Additional measurements applying *cw* laser radiation with $f = 1.63\,\mathrm{THz}$ prove that the resonance position shifts linearly with the radiation frequency as it is expected for the cyclotron resonance, see the inset in Fig. 5. The effective mass calculated from the CR is $m^* = 0.025 \cdot m_0$ being in a good agreement with the literature data on similar structures.[14, 15, 25] Momentum relaxation time determined from the resonance width ($1.1 \cdot 10^{-12}\,\mathrm{s}$) is found to be close to that obtained from the transport measurement also carried out at 4.2 K and

yielding $\tau_p = 1.3 \cdot 10^{-12}$ s.

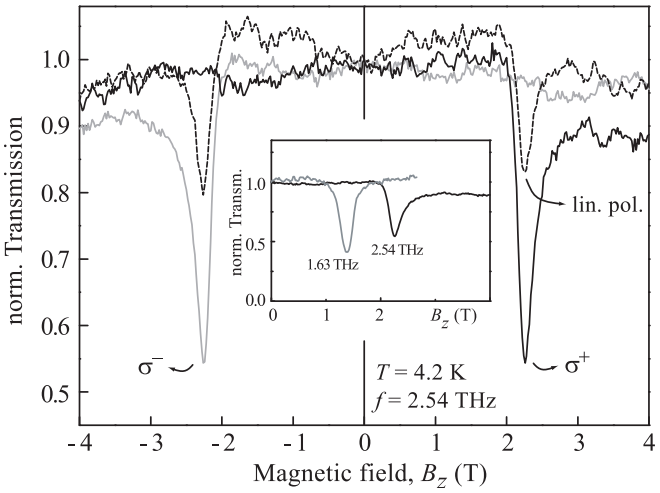

FIG. 5: Magnetic field dependence of the normalized transmission for right and left circularly as well as linearly polarized radiation at normal incidence of light. The transmitted radiation power is normalized by that at zero magnetic field. The data are obtained for $T = 4.2$ K. The inset shows transmission curves for two radiation frequencies of the *cw* laser.

SYMMETRY ANALYSIS

Photocurrents induced by homogeneous excitation of QW structures with terahertz radiation can generally be caused by photogalvanic effects (PGE), resulting from an asymmetry of the carrier photoexcitation/scattering in $\boldsymbol{k}$-space, or photon drag effects (PDE), originating from the transfer of the photon momentum $\boldsymbol{q}$ to free carriers (see e.g. [26–28]). We start with the symmetry analysis of both effects and demonstrate that the observation of the photocurrent for *s*-polarized radiation allows us to exclude PGE as a possible origin of the photocurrent and, consequently, indicates that the current is caused by the photon drag effect. PGE and PDE are phenomenologically described by equation which couples *dc* electric current with the amplitude and wave vector of the electromagnetic field inside the medium. To second order in the field amplitude (linear regime in the radiation intensity) and first order in the wave vector, such equation has the form[26, 27]

$$j_\alpha = \sum_{\beta\gamma} \chi_{\alpha\beta\gamma}(B) E_{\omega,\beta} E^*_{\omega,\gamma} + \sum_{\beta\gamma\delta} \phi_{\alpha\beta\gamma\delta}(B)\, q_\beta E_{\omega,\gamma} E^*_{\omega,\delta}\,, \tag{1}$$

where $\boldsymbol{j}$ is current density, $\boldsymbol{E}_\omega$ is the complex amplitude of the electric field of THz wave

$$\boldsymbol{E}(\boldsymbol{r},t) = \boldsymbol{E}_\omega \mathrm{e}^{i\boldsymbol{q}\cdot\boldsymbol{r}-i\omega t} + \boldsymbol{E}^*_\omega \mathrm{e}^{-i\boldsymbol{q}\cdot\boldsymbol{r}+i\omega t}\,, \tag{2}$$

$\boldsymbol{q}$ is the photon wave vector, and the indices α, β, γ, δ enumerate the Cartesian components. The third rank tensor $\chi_{\alpha\beta\gamma}$ and the forth rank tensor $\phi_{\alpha\beta\gamma\delta}$ describe the photogalvanic effects and photon drag effects, respectively. Their components may depend on static magnetic field $\boldsymbol{B}$.

Our experiments are carried out on (001)-grown quantum wells which are described by the C_{2v} point group. For these structures subjected to the magnetic field $\boldsymbol{B}$ parallel to the growth direction z, the first term in the right-hand side of Eq. (1) is given by[29]

$$\begin{aligned} j_x^{PGE} &= \chi_{xxz}(B_z) E_{\omega,x} E^*_{\omega,z} + \chi_{xyz}(B_z) E_{\omega,y} E^*_{\omega,z} + \text{c.c.} \\ j_y^{PGE} &= \chi_{yyz}(B_z) E_{\omega,y} E^*_{\omega,z} + \chi_{yxz}(B_z) E_{\omega,x} E^*_{\omega,z} + \text{c.c.}\,, \end{aligned} \tag{3}$$

where $\chi_{xxz}(B_z)$ and $\chi_{yyz}(B_z)$ are even functions of the magnetic field, $\chi_{xyz}(B_z)$ and $\chi_{yxz}(B_z)$ are odd functions, and $x \parallel [1\bar{1}0]$ and $y \parallel [110]$ are the in-plane axes. Equations (3) show that all contributions of the photogalvanic effect requires a nonzero component of the radiation electric field along the growth direction, $E_{\omega,z}$. Thus, the observation of the substantial photocurrent excited by *s*-polarized light ($E_{\omega,z} = 0$), rules out the photogalvanic effect as an origin of the observed resonant photocurrent (see inset in Fig. 1).

Now we turn to the photon drag effect described by the second term in the right-hand side of Eq. (1). Symmetry analysis shows that, in contrast to photogalvanics, photon drag effect is allowed for both *s*- and *p*-polarizations. In the case of *s*-polarized radiation and the (xz) incidence plane, i.e., for the $\boldsymbol{E}_\omega \parallel y$, the current density is given by

$$\begin{aligned} j_x^{PDE} &= \phi_{xxyy}(B_z)\, q_x |E_{\omega,y}|^2 \\ j_y^{PDE} &= \phi_{yxyy}(B_z)\, q_x |E_{\omega,y}|^2\,, \end{aligned} \tag{4}$$

where $\phi_{xxyy}(B_z)$ is an even function of the magnetic field and $\phi_{yxyy}(B_z)$ is an odd function. Consequently, we obtain that the longitudinal photocurrent (j_x) is even in the magnetic field and the transverse one (j_y) is odd. Similar results are obtained for *p*-polarized radiation.

Polarization dependence and different parity of magnetic field dependences of longitudinal and transverse photocurrent components, together with the negligible contribution of the photogalvanic effect, suggest that the photocurrent is dominated by the photon drag effect whose microscopic theory is considered in the next section.

MICROSCOPIC THEORY

We now turn to microscopic mechanisms responsible for the photocurrent generation. To that end we develop a quasi-classical theory of the cyclotron-resonance-assisted photon drag effect. Such a description is relevant to our experiments where highly doped InSb/InAlSb quantum wells with the Fermi energy about 50 meV are

exited by terahertz radiation with photon energies at least an order of magnitude smaller. In this approach, the second order response is calculated in the framework of the Boltzmann kinetic equation for the electron distribution function $f(\boldsymbol{p},\boldsymbol{r},t)$ in the momentum, coordinate, and time spaces:

$$\frac{\partial f}{\partial t}+\boldsymbol{v}\cdot\frac{\partial f}{\partial \boldsymbol{r}}+e\left(\boldsymbol{E}(\boldsymbol{r},t)+\frac{1}{c}\left[\boldsymbol{v}\times\boldsymbol{B}(\boldsymbol{r},t)\right]\right)\cdot\frac{\partial f}{\partial \boldsymbol{p}}=\mathrm{St}\left[f\right], \tag{5}$$

where $\boldsymbol{v}=\boldsymbol{p}/m^*$ is the electron velocity, e is the electron charge, $\boldsymbol{B}(\boldsymbol{r},t)=\boldsymbol{B}+\boldsymbol{B}_\omega e^{i\boldsymbol{q}\cdot\boldsymbol{r}-i\omega t}+\boldsymbol{B}^*_\omega e^{-i\boldsymbol{q}\cdot\boldsymbol{r}+i\omega t}$ is the total magnetic field consisting of the static field $\boldsymbol{B}\parallel z$ and alternating magnetic field of the THz wave with the magnitude B_ω, and $\mathrm{St}\left[f\right]$ is the collision integral.

The electric current density is given by the standard equation $\boldsymbol{j}=2e\sum_{\boldsymbol{p}}\boldsymbol{v}\,f(\boldsymbol{p},\boldsymbol{r},t)$, where a factor of 2 accounts for spin degeneracy. The *dc* photoresponse is determined by the nonequilibrium corrections to the distribution function which are proportional to $E_{\omega,\parallel}B_{\omega,z}$ and $q_\parallel E^2_{\omega,\parallel}$, where the symbol "$\parallel$" denotes the in-plane components. The terms yield two contributions to the current: (i) due to the dynamic Hall effect resulting from the joint action of electric and magnetic fields of the radiation[32] and (ii) due to spatial oscillations of the electric field and, consequently, electron distribution[33]. They were consistently considered for bulk materials[33] and two-dimensional systems with linear dispersion.[34, 35] Note that the former contribution can be also rewritten via the photon wavevector giving $q_\parallel E^2_{\omega,\parallel}$, since the amplitudes of electric and magnetic fields in the plane wave are coupled by $\boldsymbol{B}_\omega=c[\boldsymbol{q}\times\boldsymbol{E}_\omega]/\omega$. Application of the static magnetic field $\boldsymbol{B}\parallel z$, besides deflecting the current due to the Hall effect, leads to the drastic enhancement of the photon drag effect at cyclotron resonance. Estimations for the resonant photocurrent in InAs/GaSb structures is given in Ref. 39.

The details of calculations are as follows. We solve the kinetic equation Eq. (5) by expanding the distribution function $f(\boldsymbol{p},\boldsymbol{r},t)$ in the Fourier series of frequency, angular in the momentum space, and spatial harmonics

$$f=\sum_{n,m,l}f^{n,m,l}(p)\exp(-in\omega t+im\varphi_{\boldsymbol{p}}+il\boldsymbol{q}_\parallel\cdot\boldsymbol{r}), \tag{6}$$

where $\varphi_{\boldsymbol{p}}=\arctan(p_y/p_x)$ is the polar angle of the vector $\boldsymbol{p}$. Note that in thermal equilibrium, the distribution function is described by the harmonic $f^{0,0,0}(p)=\{1+\exp[(\varepsilon_p-E_F)/k_BT]\}^{-1}$, with $\varepsilon_p=p^2/(2m^*)$ being the electron energy, E_F the Fermi energy, and T the temperature, while all other harmonics vanish. For elastic or quasi-elastic electron scattering by impurities or phonons, the collision integral takes the form

$$\mathrm{St}[f]=-\sum_{n,l}\sum_{m\neq0}\frac{f^{n,m,l}(p)}{\tau_m}\exp(-in\omega t+im\varphi_{\boldsymbol{p}}+il\boldsymbol{q}_\parallel\cdot\boldsymbol{r}), \tag{7}$$

where τ_m is the relaxation time of the m-th angular harmonic of distribution function. In the Fourier series representation, Eq. (5) has the form of linear equation system for the harmonics $f^{n,m,l}(p)$

$$\begin{aligned}&\Gamma^{n,m}f^{n,m,l}-i\frac{m\,e}{cm^*}\left(B_\omega f^{n-1,m,l-1}+B^*_\omega f^{n+1,m,l+1}\right)\\&+\frac{e\boldsymbol{E}_\omega}{2}\cdot\left(\boldsymbol{o}_-\hat{K}^m_-f^{n-1,m-1,l-1}+\boldsymbol{o}_+\hat{K}^m_+f^{n-1,m+1,l-1}\right)\\&+\frac{e\boldsymbol{E}^*_\omega}{2}\cdot\left(\boldsymbol{o}_-\hat{K}^m_-f^{n+1,m-1,l+1}+\boldsymbol{o}_+\hat{K}^m_+f^{n+1,m+1,l+1}\right)\\&+i\frac{lv\boldsymbol{q}_\parallel}{2}\left(\boldsymbol{o}_-f^{n,m-1,l}+\boldsymbol{o}_+f^{n,m+1,l}\right)=0\,,\end{aligned} \tag{8}$$

where $\Gamma^{n,m}=1/\tau_m-in\omega-im\omega_c$, $\omega_c=eB_z/(m^*c)$ is the cyclotron frequency, $\boldsymbol{o}_\pm=\boldsymbol{o}_x\pm i\boldsymbol{o}_y$, $\boldsymbol{o}_x$ and $\boldsymbol{o}_y$ are the unit vectors along x and y, respectively, $\hat{K}^m_\pm=\partial_p\pm(m\pm1)/p$. Straightforward calculations show that, for $\boldsymbol{q}_\parallel\|x$ and degenerate electron gas, the components of the drag current density have the form

$$j^{\mathrm{pd}}_x=\mathrm{Re}(\tilde{j})\,,\quad j^{\mathrm{pd}}_y=-\,\mathrm{Im}(\tilde{j})\,, \tag{9}$$

where

$$\begin{aligned}\tilde{j}=&\frac{q_\parallel e^3|E_{\omega,\parallel}|^2\,n_s}{\omega m^{*2}}\frac{\tau_p}{1-i\omega_c\tau_p}\sum_\pm\left\{\tau_p\frac{1\pm\xi_3}{1+(\omega\pm\omega_c)^2\tau_p^2}\right.\\&+\frac{1}{2}\frac{\tau'_pE_F}{1-i\omega_c\tau_p}\left[\left(\frac{\xi_1-i\xi_2}{1+i(\pm\omega-\omega_c)\tau_p}+\frac{1\pm\xi_3}{1+i(\pm\omega+\omega_c)\tau_p}\right)\right.\\&\left.\left.\pm\frac{i\omega\tau_2(1\mp\xi_3)}{[1+i(\pm\omega-2\omega_c)\tau_2][1+i(\pm\omega-\omega_c)\tau_p]}\right]\right\},\end{aligned} \tag{10}$$

$n_s=m^*E_F/(\pi\hbar^2)$ is the electron density, $\tau_p\equiv\tau_1$ is momentum relaxation time, $\tau'_p=d\tau_p(E_F)/dE_F$, parameters ξ_1, ξ_2, and ξ_3 are determined by polarization state of radiation and connected to the Stokes parameters.[36] The parameters are given by $\xi_1=(|E_{\omega,x}|^2-|E_{\omega,y}|^2)/E^2_{\omega,\parallel}$, $\xi_2=(E_{\omega,x}E^*_{\omega,y}+E^*_{\omega,x}E_{\omega,y})/E^2_{\omega,\parallel}$, and $\xi_3=i(E_{\omega,x}E^*_{\omega,y}-E^*_{\omega,x}E_{\omega,y})/E^2_{\omega,\parallel}$, the latter one reflecting the radiation helicity. Equation (10) shows that the photon drag current consists of two contributions: one being proportional to τ_p (first term in the curly brackets) and the other to the first derivative τ'_p. It is remarkable that, while the first contribution exhibits the resonance at CR, i.e., for $\omega=\omega_c$, the second one has an additional resonance at the double frequency, $\omega=2\omega_c$, where the radiation absorption does exhibit this peculiarity. Dependence of the drag current on the polarization parameters ξ_1 and ξ_2 in two-dimensional systems with parabolic energy spectrum arises to the extent of energy dependence of the momentum relaxation time. At the same time, the strong dependence of the photocurrent on radiation helicity results from the circular dichroism of the cyclotron-resonance absorption.

Finally, for the case of weak energy dependence of the momentum relaxation time, i.e., $\tau_p' \ll \tau_p/E_F$, which is relevant for short-range scattering,[37] and linearly polarized radiation, Eq. (10) reduces to

$$j_x^{\rm pd} = \frac{q_\parallel e^3 |E_{\omega,\parallel}|^2 n_s}{\omega m^{*2}} \frac{\tau_p^2}{1+(\omega_c\tau_p)^2} \sum_{\pm} \frac{1}{1+(\omega \pm \omega_c)^2\tau_p^2} ,$$
$$j_y^{\rm pd} = -\omega_c\tau_p j_x^{\rm pd} . \qquad (11)$$

In the next section we analyze this result, compare it with experimental data and show that it describes well all experimental findings.

DISCUSSION

The above theory is developed in the assumption of a weak electron gas heating which is relevant to our experiments applying low-power radiation of the *cw* laser. In these measurements, the corresponding photocurrents have been detected by the voltage drops, $U_{x,y}$, picked up across a 1 MΩ load resistors being much larger than the resistance of the QW structures. To obtain $U_{x,y}$ from Eq. (11) we find the steady-state distribution of the electric potential $\Phi(r)$ by solving the continuity equation $\mathrm{div}\, \boldsymbol{j} = 0$ with boundary conditions setting the zero electric current across the sample edges. Here the total electric current, $\boldsymbol{j}$, is written in the form

$$j_\alpha = j_\alpha^{\rm pd} - \sum_{\beta=x,y} \sigma_{\alpha\beta}\nabla_\beta\Phi , \qquad (12)$$

where $j_\alpha^{\rm pd}$ is the local current density given by Eq. (11), the second term describes the drift current, $\sigma_{xx} = \sigma_{yy} = \sigma_0/[1+(\omega_c\tau_p)^2]$, $\sigma_{xy} = \sigma_{yx} = -\omega_c\tau_p\sigma_0/[1+(\omega_c\tau_p)^2]$ are the components of the conductivity tensor in a static magnetic field, $\sigma_0 = ne^2\tau_p/m^*$ is the zero-field conductivity.

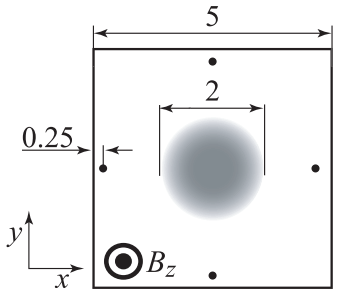

FIG. 6: Sample and contact dimensions in millimeters. Gray circle shows the laser spot located in the center of the sample. The spot has the Gaussian profile of about 2 mm diameter. Voltage drops U_x and U_y are measured between opposite contacts.

Figures 7 and 8 show calculated dependences of the photovoltages $U_{x,y}$ on the magnetic field. The calculations are carried out for the momentum relaxation time, $\tau_p = 1.1\cdot 10^{-12}$ s and the effective mass $m^* = 0.025\cdot m_0$ both obtained by the transmission measurements, the incidence angle $\theta_0 = 20°$; the sample dimensions, the position of the contacts[38] and the Gaussian laser beam profile are shown in Fig.6. Comparison of the results of Figs. 7 and 8 with the corresponding experimental data shown in Figs. 1 and 2 demonstrates that all essential features of the observed photocurrent are well described by the microscopic model of the cyclotron-resonance-assisted photon drag effect. In particular, for linearly polarized radiation, U_y and U_x are described by the odd and even functions of the magnetic field. Estimations of the photovoltage magnitude, carried out after Eqs. (11) and (12) and using parameters determined from the transport and CR transmission measurements, yield $U_x = 0.05\,\mathrm{mV/W}$ for degenerate 2DEG, which is in good agreement with the value obtained in the experiments. Both the theory and experiment show that the photocurrent at the cyclotron resonance is enhanced by more than 50 times as compared to the one excited at zero field, Figs. 1, 2, 7, and 8. Note, that in another narrow band material, InAs/GaSb QWs, only a weak resonance with an amplitude comparable to that at zero magnetic field has been detected.[39]

Solution of Eq. (12) with currents given by Eqs. (11) allows us to fit photovoltage data and obtain the momentum relaxation times which found to be equal to $0.9\cdot 10^{-12}$ and $0.7\cdot 10^{-12}$ s for $T = 50$ and 80 K, respectively. The former value and the reduction of the relaxation time with the temperature increase are in a good agreement with the magneto-transport measurements. Moreover, our data provide even deeper insight in the scattering mechanisms. Indeed, the experimental data are well described by the calculations after Eqs. (11) and (12) obtained assuming a weak energy dependence of the momentum relaxation time, i.e., $\tau_p' \ll \tau_p/E_F$. The validity of this assumption manifests itself in the magnetic field dependence of the photocurrent, see Figs. 1 and 2, which does not show any peculiarities at $B = B_c/2$ at which for the opposite unequality an additional resonance should appear, see Eqs. (10).

Finally, the calculations show that the amplitudes of the resonance are nearly the same for *s*- and *p*-polarized radiation, which agrees well with experimental findings, see Figs. 1 and 2. Indeed, the polarization dependence of the photon drag current for energy-independent relaxation time is described by $|E_{\omega,\parallel}|^2$, see Eqs. (11), which for *s*- and *p*-polarizations are given by $|E_{\omega,\parallel}|^2 = 2\pi t_s^2 I_0/c$ and $|E_{\omega,\parallel}|^2 = 2\pi t_p^2 I_0\cos^2\theta/c$, respectively. Here, t_s and t_p are the amplitude transmission coefficients for *s*- and *p*-waves, I_0 is the radiation intensity, θ is the angle of refraction related with the incidence angle θ_0 by $\sin\theta = \sin\theta_0/n_\omega$, and n_ω is the refraction index. Consequently, for small angles of incidence with $\cos\theta \approx 1$ and $t_p \approx t_s$, the fields $|E_{\omega,\parallel}|$ and the resulting photocurrents are close to each other for the considered polarization

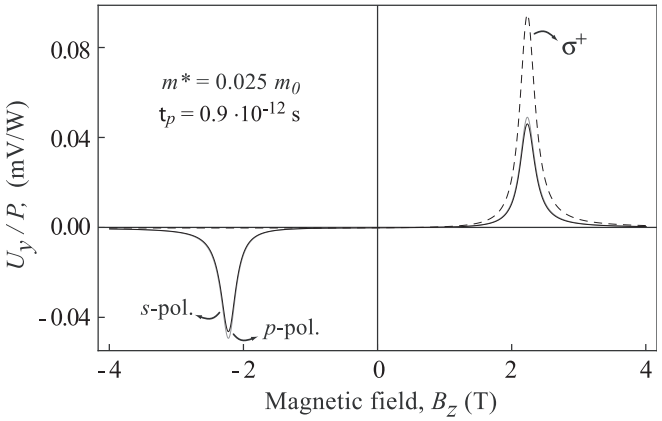

FIG. 7: Theoretical dependences of U_y/P on magnetic field for s-, p- and σ^+-polarizations.

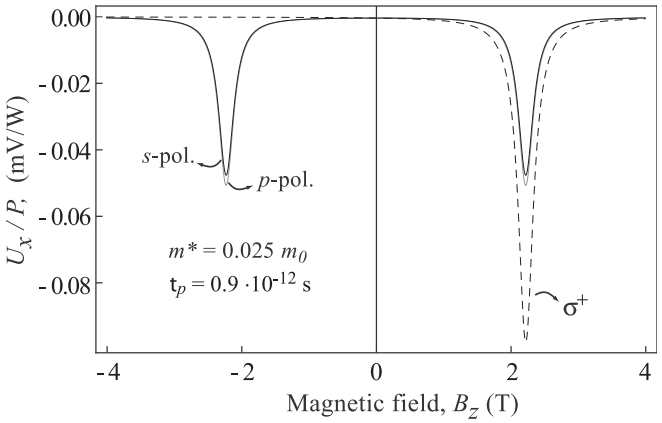

FIG. 8: Theoretical dependences of U_x/P on magnetic field for s-, p- and σ^+-polarizations.

states. Figures 7 and 8 also show the photocurrent excited by right-handed, σ^+, circularly polarized radiation. It is seen that, as expected for CR, here the resonant signal is generated for one magnetic field polarity only (positive B_z) and that its magnitude is enhanced by factor 2 compared to that excited by linearly polarized radiation.

Now we briefly address the observed oscillations of the photocurrent. The oscillations have been detected at low temperature and applying *cw* laser radiation only. They correlate with the Shubnikov – de Haas oscillations and vanish at high lattice or electron temperature. The latter has been proved applying pulsed high power radiation resulting in a strong electron gas heating, which manifests itself in the substantial photoconductive signal.[27] In this particular case, even at $T = 4.2$ K we only detected the resonant photocurrent. The correlation with SdH indicates that the resonances are caused by periodic modification of the electron scattering, however the detailed mechanism of the oscillating photocurrent remains unclear and requires further experimental and theoretical studies. In particular, the observed two times difference in the oscillation frequencies should be explored.

SUMMARY

Our observations demonstrate that in InSb/InAlSb QWs the photon drag effect resulting from the transfer of photon momentum to free electrons is strong under cyclotron resonance conditions. The microscopic theory of the photon drag effect in two-dimensional electron systems with parabolic energy spectrum developed in the framework of Newton equations of motion and Boltzmann kinetic equation for the distribution function describes well all experimental findings. The observed effect provides complimentary method to study details of the band structure and carrier dynamic in InSb-based two dimensional structures. In particular, almost identical Lorentz profiles and the resonance positions observed in the experiments on photocurrent excited by low power THz excitation and radiation transmission, demonstrate, that the photon drag effect can be applied for measuring of the effective mass. Since a large photoresponse is observed at high temperatures and should also yield well detected signals for the structures with a low carrier density, this method can be used even under the conditions where transmission signals are unresolvable. Furthermore, our analysis shows that investigating the resonance photocurrent at magnetic fields equal to a half of B_c one can study the energy dependence of the momentum relaxation time, gaining information not easily accessible by other experimental methods.

The financial support from the DFG (SFB 689), the Linkage Grant of IB of BMBF at DLR, and RFBR, is gratefully acknowledged.

[1] Ashley T, Buckley L, Datta S, Emeny M T, Hayes D G, Hilton K P, Jefferies R, Phillips T J, Wallis D J, Wilding P J and Chau R 2007 Hetergeneous InSb quantum well transistors on silicon for ultra-high speed, low power logic application *Electron. Lett.* **43**, 14

[2] Gilbertson A M, Kormányos A, Buckle P D, Fearn M, Ashley T, Lambert C J, Solin S A and Cohen L F 2011 Room temperature ballistic transport in InSb quantum well nanodevices *Appl. Phys. Lett.* **99**, 242101

[3] Gilbertson A M, Fearn M, Kormányos A, Read D E, Lambert C J, Emeny M T, Ashley T and Solin S A 2011 Ballistic transport and boundary scattering in InSb/$In_{1-x}Al_xSb$ mesoscopic devices *Phys. Rev.* B **83**, 075304

[4] Goel N, Graham J, Keay J C, Suzuki K, Miyashita S, Santos M B and Hirayama Y 2005 Ballistic transport in InSb mesoscopic structures *Physica* E **26**, 455

[5] Gilbertson A M, Fearn M, Jefferson J H, Murdin B N, Buckle P D and Cohen L F 2008 Zero-field spin splitting and spin lifetime in n-InSb/$In_{1-x}Al_xSb$ asymmetric quantum well heterostructures *Phys. Rev.* B **77**, 165335

[6] Gilbertson A M, Branford W R, Fearn M, Buckle L, Buckle P D, Ashley T and Cohen L F 2009 Zero-field spin splitting and spin-dependent broadening in high-mobility InSb/$In_{1-x}Al_xSb$ asymmetric quantum well heterostructures *Phys. Rev.* B **79**, 235333

[7] Khodaparast G A, Meyer R C, Zhang X H, Kasturiarachchi T, Doezema R E, Chung S J, Goel N, Santos M B and Wang Y J 2004 Spin effects in InSb quantum wells *Physica* E **20**, 386

[8] Frazier M, Waugh J A, Heremans J J, Santos M B, Liu X and Khodaparast G A 2009 Photoinduced spin-polarized current in InSb-based structures *J. Appl. Phys.* **106**, 103513

[9] Stachel S, Olbrich P, Zoth C, Hagner U, Stangl T, Karl C, Lutz P, Bel'kov V V, Golub L E, Clowes S K, Ashley T, Gilbertson A M and Ganichev S D 2012 Interplay of spin and orbital magnetogyrotropic photogalvanic effects in InSb/AlInSb quantum well structures *Phys. Rev.* B **85**, 045305

[10] Li J, Gilbertson A M, Litvinenko K L, Cohen L F and Clowes S K 2012 Observation of spin dependent photoconductivity in InSb quantum well nanowires *Appl. Phys. Lett.* **101**, 152407

[11] Li J, Gilbertson A M, Litvinenko K L, Cohen L F and Clowes S K 2012 Transverse focusing of spin-polarized photocurrents *Phys. Rev.* B **85**, 045431

[12] Ganichev S D and Ivchenko E L 2008 *Spin Photogalvanics*, in *Spin Physics in Semiconductors*, Ed. M. I. Dyakonov (Berlin: Springer)

[13] Seeger K 1985 *Semiconductor Physics* (Berlin and Heidelberg: Springer)

[14] Orr J M S, Chuang K-C, Nicholas R J, Buckle L, Emeny M T and Buckle P D 2009 Magnetoabsorption in InSb quantum-well heterostructures *Phys. Rev.* B **79**, 235302

[15] Khodaparast G A, Larrabee D C, Kono J, King D S, Chung S J and Santos M B 2003 Relaxation of quasi-two-dimensional electrons in a quantizing magnetic field probed by time-resolved cyclotron resonance *Phys. Rev.* B **67**, 035307

[16] Gouider F, Vasilyev Yu B, Bugár M, Könemann J, Buckle P D and Nachtwei G 2010 Terahertz photoresponse of AlInSb/InSb/AlInSb quantum well structures *Phys. Rev.* B **81**, 155304

[17] Kvon Z D, Danilov S N, Mikhailov N N, Dvoretsky S A, and Ganichev S D 2008 Cyclotron resonance photoconductivity of a two-dimensional electron gas in HgTe quantum wells *Physica E* **40**, 1885

[18] Ziemann E, Ganichev S D, Yassievich I N, Perel V I and Prettl W 2000 Characterization of deep impurities in semiconductors by terahertz tunneling ionization *J. Appl. Phys.* **87**, 3843

[19] Ganichev S D, Emel'yanov S A and Yaroshetskii I D 1982 Spectral sign inversion of photon drag at far-IR wavelengths *Pisma Zh. Eksp. Teor. Fiz.* **35**, 297 [*JETP Lett.* **35**, 368]

[20] Ganichev S D, Diener J, Yassievich I N, Prettl W, Meyer B K and Benz K W 1995 Tunnelling ionization of autolocalized DX- centers in terahertz fields Phys. Rev. Lett. **75**, 1590

[21] Ganichev S D, Terent'ev Ya V and Yaroshetskii I D 1985 Photon-drag photodetectors for the far-IR and submillimeter regions *Pisma Zh. Tekh. Fiz* **11**, 46 [*Sov. Tech. Phys. Lett.* **11**, 20]

[22] Note that at normal incidence the signal is not detected for any magnetic field strength.

[23] Pooley O J, Gilbertson A M, Buckle P D, Hall R S, Buckle L, Emeny M T, Fearn M, Cohen L F and Ashley T 2010 Transport effects in remote-doped InSb/$Al_xIn_{1-x}Sb$ heterostructures *New J. Phys.* **12**, 053022

[24] Gilbertson A M, Buckle P D, Emeny M T, Ashley T and Cohen L F 2011 Suppression of the parasitic buffer layer conductance in InSb/$Al_xIn_{1-x}Sb$ heterostructures using a wide-band-gap barrier layer *Phys. Rev.* B **84**, 075474

[25] Nedniyom B, Nicholas R J, Emeny M T, Buckle L, Gilbertson A M, Buckle P D and Ashley T 2009 Giant enhanced g-factors in an InSb two-dimensional gas *Phys. Rev.* B **80**, 125328

[26] Ivchenko E L 2005 *Optical Spectroscopy of Semiconductor Nanostructures* (Harrow: Alpha Science)

[27] Ganichev S D and Prettl W 2006 *Intense Terahertz Excitation of Semiconductors* (Oxford: Oxford University Press)

[28] Ganichev S D, Ivchenko E L, and Prettl W, Photogalvanic effects in quantum wells 2002 *Physica E* **14**, 166

[29] Note that generally speaking in the presence of magnetic field the photocurrent may also be generated by magneto gyrotropic photogalvanic effect.[30] However, for the point group C_{2v} this effect vanishes for $\boldsymbol{B} \parallel z$ [31] and therefore is disregarded in the further consideration.

[30] Bel'kov V V, Ganichev S D, Ivchenko E L , Tarasenko S A, Weber W, Giglberger S, Olteanu M, Tranitz H-P, Danilov S N, Schneider Petra, Wegscheider W, Weiss D and Prettl W 2005 Magneto-gyrotropic photogalvanic effects in semiconductor quantum wells *J. Phys. C: Condens. Matter* **17**, 3405

[31] Bel'kov V V and Ganichev S D 2008 Magneto-gyrotropic effects in semiconductor quantum wells *Semicond. Sci. Techn.* **23**, 114003

[32] Barlow H M 1954 Application of the Hall effect in a semiconductor to the measurement of power in an electromagnetic field *Nature* **173**, 41

[33] Perel V I and Pinskii Ya M 1973 Constant current in conducting media due to a high-frequency electron electromagnetic field *Sov. Phys. Solid State*, **15**, 688

[34] Karch J, Olbrich P, Schmalzbauer M, Zoth M, Brinsteiner C, Fehrenbacher M, Wurstbauer U, Glazov M M, Tarasenko S A, Ivchenko E L, Weiss D, Eroms J, Yakimova R, Lara-Avila S, Kubatkin S and Ganichev S D 2010 Dynamic Hall Effect Driven by Circularly Polarized Light in a Graphene Layer *Phys. Rev. Lett.* **105**, 227402

[35] Glazov M M and Ganichev S D 2013 High frequency electric field induced nonlinear effects in graphene *Physics Reports* http://dx.doi.org/10.1016/j.physrep.2013.10.003

[36] Saleh B E A and Teich M C 2003 *Fundamentals of Photonics* (New York: John Wiley & Sons)

[37] The absence of a noticeable energy dependence of the relaxation time τ_p is additionally supported by the fact that no resonant photocurrent is observed at $\omega = 2\omega_c$ which is expected from Eq. (10) elsewise.

[38] Note that while the longitudinal voltage, U_x, is nearly independent of distance between contact and sample edge the transverse one, U_y, is sensitive to the contact positions.

[39] Dmitriev A P, Emelyanov S A, Ivanov S V, Kop'ev P S, Terent'ev Ya V and Yaroshetsky I D 1991 Drag photocurrent in a 2D electron gas near the cyclotron resonance and its first subharmonic *Pisma Zh. Eksp. Teor. Fiz.* **54**, 460

(1991) [*JETP Lett.* **54**, 462]